Building and Environment 90 (2015) 15–29

Contents lists available at ScienceDirect

Building and Environment

journal homepage: www.elsevier.com/locate/buildenv

Effect of urban neighborhoods on the performance of building cooling systems

Stefan Gracik [a], Mohammad Heidarinejad [a, b], Jiying Liu [c], Jelena Srebric [a, b, *]

[a] Department of Mechanical Engineering, The Pennsylvania State University, University Park, PA 16802, USA
[b] Department of Mechanical Engineering, University of Maryland, College Park, MD 20742, USA
[c] School of Thermal Engineering, Shandong Jianzhu University, Jinan 250101, China

ARTICLE INFO

Article history:
Received 27 December 2014
Received in revised form
26 February 2015
Accepted 27 February 2015
Available online 12 March 2015

Keywords:
Urban microclimate
Efficiency of building cooling systems
Building energy consumption
Computational fluid dynamics
Building energy simulations

ABSTRACT

This paper quantified the influence of the urban neighborhood on the degradation of Coefficient of Performance (COP) for the building cooling systems. Urban microclimate usually creates higher air temperatures in dense urban areas compared to surrounding rural and suburban regions. Computational Fluid Dynamics (CFD) combined with building energy simulations can predict local hourly temperatures in urban environments. This study uses open source software packages, including OpenFOAM and EnergyPlus, to calculate local air temperatures and heat fluxes on the building surfaces as well as resultant operational COP values. First, the simulated temperature calculations of local airflow temperatures are indirectly validated using on-site field measurements in an actual urban neighborhood. Further, the validated CFD simulations predicted local air temperatures in uniform neighborhoods of varying density. This study identified four types of COP equations to quantify performance of cooling systems as a function of outdoor air temperatures. The study findings indicate that for the present study's climate and flow conditions, rooftop air conditioners in urban areas can have a reduction in COP up to 17%, compared to COP in a corresponding rural area. Window air conditioners can have reductions in COP of over 16%, if located on the windward walls. However, this average COP degradation for the cooling systems installed on the leeward walls is not significant. Overall, the effect of neighborhoods on the performance of cooling systems is significant and quantifiable, and this quantification requires consideration of the common local design practices for the installation of building cooling systems.

1. Introduction

The rapidly urbanizing world is causing drastic changes to global energy use patterns. At the beginning of the 20th century, 13 percent of the world's population lived in urban areas. Today, over 50 percent reside in urban areas [1]. This continued urbanization is exasperating the Urban Heat Island (UHI) effect, which affects the microclimate of cities. The UHI effect is partially due to the thermal properties of common building materials and heat transfer among building surfaces in the built environment [2]. For example, the building materials with high solar energy absorption cause high surface temperatures leading to warming of the surrounding air. This increase in the local air temperatures due to UHI exacerbates the existing demand to cool buildings. Therefore, there is a need to quantify the additional demand on cooling equipment capacity due to the increase in the surrounding local air temperature and ultimately degradation in the efficiency of the building cooling systems.

Numerous studies have considered different aspects of the urban neighborhood influence and ultimately UHI on energy consumption of the buildings and the implication of the changes in the local thermo-fluid properties on the modeling of the buildings. For example, existing studies explored the influence of the UHI on the cooling demand of the buildings [3,4], energy consumption of the buildings [3,5,6], local temperature increase [7,8], air velocity variations [9], Convective Heat Transfer Coefficients (CHTCs) [10–12], as well as short- and long-wave solar radiation [13,14]. However, these existing studies did not examine the impacts of the UHI and urban neighborhood on the performance degradation of the Heating, Ventilating and Air-Conditionings (HVAC) systems.

* Corresponding author. Department of Mechanical Engineering, University of Maryland, College Park, MD 20742, USA. Tel.: +1 (301) 405 7276; fax: +1 (301) 314 9477.
E-mail address: jsrebric@umd.edu (J. Srebric).

http://dx.doi.org/10.1016/j.buildenv.2015.02.037
0360-1323/

Therefore, this study considers the impacts of the local urban neighborhood on the thermo-fluid properties of the airflow and temperature fields and their implications on the degradation of the cooling system efficiencies.

In actual buildings, efficiency of the HVAC systems directly depends on outdoor air temperature with the increase in local temperatures resulting in the decrease of building HVAC systems efficiency. For the theoretical reverse cycle, Carnot efficiency shows that the Carnot cycle's efficiency decreases with increasing the hot reservoir temperature. Previous studies have emphasized the diurnal changes in the Coefficient of Performance (COP) of the HVAC system [15,16]. However, these studies did not fully examine the link between the impacts of the urban neighborhood on the local air temperature and corresponding degradation of the cooling systems. Computational Fluid Dynamics (CFD) is a reliable tool to calculate the local spatial and temporal temperatures in urban environments that requires previous backgrounds in the outdoor simulations [17,18]. Therefore, this study utilizes CFD to predict the flow field around the building of interest and calculate the diurnal changes in the COP of HVAC systems due to the local urban neighborhood characteristics.

Several existing CFD studies calculated local temperatures, and these studies used a variety of methods to define appropriate thermal boundary conditions [19–21]. A few studies have also applied CFD to estimate the local temperatures and corresponding COP of HVAC systems [22–26]. These COP studies focused on the temperature stratification for high-rise buildings, rather than the elevated temperatures due to urban density. Therefore, this study aims to utilize the existing empirical COP equations with validated building airflow and energy simulation models to quantify changes in the COP of cooling systems.

In the interest of making the research results accessible to a large audience of users, it is advantageous to use open source simulation software. The performance of OpenFOAM open source CFD software has been shown to be capable of providing validated results for isothermal urban environments [27]. This study provides an indirect validation of the OpenFOAM simulation results in non-isothermal environments with on-site field measured data to assess the accuracy of predicted local temperatures for an actual urban neighborhood with urban plan area density of 0.25. Urban plan area density (λ_p) is the ratio of the built area projected onto the ground surface divided by the total land area under consideration. In addition, this study developed an open source simulation framework using OpenFOAM and EnergyPlus to calculate local temperatures in urban neighborhoods. A comparison between CFD and measured temperature data collected at the Penn State campus served as a validation study for the developed framework. This study benefited from a validation method that was previously published to indirectly validate the outdoor CFD simulation results [12]. Finally, the developed CFD simulations for neighborhoods with varying plan area densities enabled calculations of the change in COP for highly dense urban neighborhoods.

Overall, the reduction in efficiency of cooling systems due to urban density is an important parameter when considering future infrastructure investments for urban neighborhoods. This study assesses the degradation of COP while it considers the following criteria:

(1) Make consistent decision-making regarding CFD case study setup for urban neighborhoods using systematic consideration of the boundary conditions, mesh generation, and inputs.
(2) Deploy open source software for simulations, including OpenFOAM for the CFD simulations, EnergyPlus for the building energy simulations, and ParaView for the visualization of the outputs.
(3) Establish best practices for handling the thermal boundary conditions of urban neighborhoods based on validation of the CFD simulations with the on-site measured data.
(4) Quantify the effect of urban density on the efficiency of cooling systems due to local thermal conditions by utilizing the existing COP equations for actual operating conditions of HVAC systems.

2. Research methodology

The research methodology includes details about the modeling procedure and inputs for CFD and energy simulations to evaluate the impacts of the urban neighborhood on the performance of the HVAC systems [28].

2.1. Modeling procedure

This study used CFD and building energy simulations to develop a framework, enabling evaluation of the influence of the urban neighborhood on building cooling systems. Fig. 1 illustrates the developed framework in this study. First, this study assessed the effectiveness of the proposed framework with the validation of the simulation results for an actual urban neighborhood in a non-isothermal environment. Then, this study extended the applicability of the framework to hypothetical buildings located in six different urban neighborhood densities. This framework used the open source packages to perform the simulations, EnergyPlus and OpenFOAM. Any simulation engines or models with proprietary access are not included in this study. The airflow simulations with OpenFOAM have validation for isothermal conditions in urban neighborhoods [27]. The building energy simulations with EnergyPlus provide validated thermal behavior of the building envelope and its HVAC systems throughout a year [29]. Simulation results from EnergyPlus supplied OpenFOAM with building surface temperatures/fluxes as the boundary conditions, while CFD simulations provided convective heat transfer into the atmosphere at external building surfaces [11]. SketchUp with the OpenStudio plugin produced building geometry in the STL (STereoLithography) format for OpenFOAM, as well as the IDF (Input Dictionary File) format for EnergyPlus. To simplify the computational framework, the building energy and CFD simulations ran in parallel with hourly exchange of data from EnergyPlus to OpenFOAM.

2.2. Description of the selected urban neighborhoods

The validation study uses an actual urban neighborhood with measured data for four buildings located at Penn State's campus neighborhood. The buildings are 10 stories tall, and measure 20 m × 30 m × 28 m. The short surfaces of the buildings have a Window-to-Wall (WWR) ratio of 0.15, and the long surface WWR is 0.2. The actual urban neighborhood has a plan area density of 0.25. Due to the existence of low WWR for the selected buildings, this study used the existing methods in EnergyPlus to calculate the solar radiation that encompasses both long-wave and short-wave radiation. The further study included neighborhoods with six different plan area densities, 0.04, 0.063, 0.11, 0.16, 0.25, and 0.44, corresponding to a building spacing ranging from 5 m to 40 m. These urban densities represent sparse rural/suburb areas ($\lambda_p = 0.04$) up to dense city centers ($\lambda_p = 0.44$). Fig. 2 illustrates two different plan area densities and position of the building of interest in the center. Previous roughness studies established that flow fields over arrays of cubes experience three different airflow regimes [30]. In the lowest density arrays, each cube is largely isolated from the effects of the other cubes. In the middle density

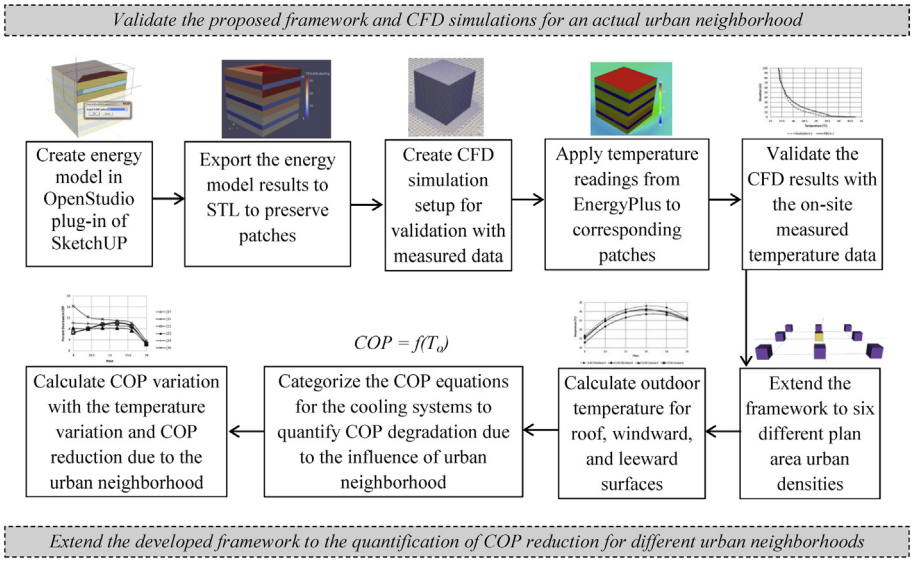

Fig. 1. Workflow of the proposed modeling framework to couple airflow and energy simulations for urban neighborhoods.

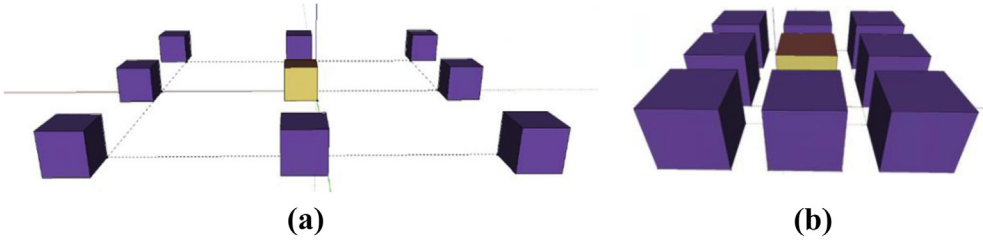

Fig. 2. Representation of building arrays with the central position for the building of interest and two extreme plan area densities λ_p (a) 0.04 and (b) 0.44.

arrays, the wake created by a cube begins to interfere with the flow over cubes downstream from it. For the highest density arrays, the flow begins to skim across the tops of the cubes, minimizing the mixing of the fluid in between the cubes with the free stream airflow.

2.3. CFD and energy governing equations

In order to accurately predict the local temperatures in urban neighborhoods, the energy balance equations need to account for both heat transfer processes occurring in the building envelope, and the transport of thermal energy by fluid motion [19,29]. The calculations for building envelope take into account indoor air temperature, solar radiation, and convection. These heat transfer processes result in a time dependent lag between solar radiative forcing, and building surface temperature/flux. For an accurate simulation of building surface temperatures, the chosen methodology should also account for the most significant heat transfer processes within a building [31]. Finally, this study uses the existing empirical COP correlations for modeling performance of the building cooling systems with the environmental conditions within the studied urban neighborhoods.

The EnergyPlus simulations calculate the energy balance both internally in the building and at its external surfaces. The external surface fluxes and corresponding temperatures use the outside surface energy balance equation defined as follows [32]:

$$q''_{\alpha sol} + q''_{LWR} + q''_{conv} - q''_{ko} = 0 \tag{1}$$

where $q''_{\alpha sol}$ is the absorbed solar radiation, q''_{LWR} is the estimated net long-wave radiation, q''_{conv} is the net heat transfer due to the outdoor air via convection, and q''_{ko} is the heat transferred through the building envelope. It is important to note that this study uses the existing methods in EnergyPlus to calculate different heat fluxes. For the selected urban neighborhoods in this study, the EnergyPlus methods provide satisfactory performance [29]. Although there are software packages able to provide accurate representation of different terms in this equation, based on the scope of this study, the existing open source software packages and models are connected and used.

For the conduction heat transfer through the building envelope, the EnergyPlus simulations use Conduction Transfer Functions (CTFs) to provide the analytical solutions. Additionally, the present study employs the interactions between spatial distribution of the temperatures on the building surfaces, ground, and sky using the view factor method to account for the short-wave and long-wave radiations [32]. Surrounding objects, such as neighboring buildings, create shadows to emulate the solar conditions for a range of neighborhood densities. The following equation represents the convective heat transfer:

$$Q_c = h_{c,ext} A \left(T_{surf} - T_{air} \right) \tag{2}$$

where $h_{c,ext}$ represents the convective heat transfer coefficients, A represents the fluid-solid contact area through which heat flows, T_{surf} represents the building wall surface temperatures, and T_{air} represents the air temperatures adjacent to the building. This study employs the DOE2 algorithm for calculations of convective heat transfer coefficients in the EnergyPlus [32], which states that for natural and smooth forced convection:

$$h_n = \frac{A|\Delta T|^{\frac{1}{3}}}{B - cos\Sigma} \tag{3}$$

where A and B are constants that depend on the orientation of the body (horizontal or vertical) and whether the surface temperature is greater than or less than the temperature of its surroundings. Another approach is to exchange the calculated CHTC from the CFD simulations to the energy simulations. Existing studies have considered this influence for different building types [12,29]. Furthermore, $|\Delta T|$ represents the difference between building surface temperature and outdoor air temperature. The equation for forced convection on smooth surfaces, such as glass, is:

$$h_{c,glass} = \left(h_n^2 + \left[aV_z^b\right]^2\right)^{\frac{1}{2}} \tag{4}$$

where a and b are constants depending on the orientation of the building surface (windward or leeward direction). For rough surfaces, an additional equation provides the convection coefficients:

$$h_c = h_n + R_f\left(h_{c,glass} - h_n\right) \tag{5}$$

where R_f is a roughness multiplier varying from 1.0 for smooth surfaces to 2.17 for very rough surfaces.

For the CFD simulations, the buoyancy force calculations use the Boussinesq assumption, resulting in the following equations that govern the fluid velocity and temperature:

$$\frac{\partial u_i}{\partial x_i} = 0 \tag{6}$$

$$\frac{\partial}{\partial x_i}\left(u_i u_j\right) = -\frac{1}{\rho}\frac{\partial p_{\rho gh}}{\partial x_i} + \frac{\partial}{\partial x_j}\left[\nu\left(\frac{\partial u_i}{\partial x_j} + \frac{\partial u_j}{\partial x_i}\right) - \overline{u_i' u_j'}\right] - \rho_o g_i \beta\left(T - T_{ref}\right) \tag{7}$$

$$u_j\frac{\partial T}{\partial x_j} = \frac{\partial}{\partial x_j}\left[\alpha\frac{\partial T}{\partial x_j} - \rho c\left(\overline{\nu' T'}\right)\right] \tag{8}$$

where u is the velocity, ν is the kinetic viscosity, $-\rho u_i' u_j'$ is the Reynolds Stress, β is thermal expansion, T is the temperature, and $p_{\rho gh}$ is equal to $p - \rho gz$. This study uses an eddy viscosity model to approximate the Reynold's stress tensor:

$$u_i' u_j' = \nu_t\frac{\partial u}{\partial x_i} \tag{9}$$

where ν_t is the eddy viscosity. Specifically, the present study uses the two equation $k-\varepsilon$ models to estimate the eddy viscosity as $\nu_t = C_u\frac{k^2}{\varepsilon}$, where k is the turbulent kinetic energy, ε is the turbulent dissipation, and C_u is a constant set to 0.0845. For the temperature field, turbulent thermal diffusivity is approximated as $\alpha_t = \nu_t/Pr_t$, where Pr_t is the turbulent Prandtl number, approximated as an average of 0.8 in this study. In this study, $u(z)$ for the inlet is defined by the following equations [33]:

$$u(z) = \frac{u^*}{\kappa}\ln\left(\frac{z - z_g + z_o}{z_o}\right) \tag{10}$$

$$u^* = \kappa\frac{U_{ref}}{\ln\left(\frac{z_{ref} + z_o}{z_o}\right)} \tag{11}$$

$$\varepsilon = \frac{u^{*3}}{\kappa(z + z_o)} \tag{12}$$

where u^* is the friction velocity, z is the elevation above the ground, z_g is the elevation of the ground, z_o is the roughness length of the ground, and κ is the Von Karman constant ($\kappa = 0.41$). For this study z_o is 0.3m due to existence of small obstacles in the studied neighborhoods.

2.4. CFD and energy boundary conditions

The CFD analysis in the present study followed previous recommendations for case setup set by AIJ [34], COST [27], as well as OpenFOAM specific recommendations by Franke [35]. The domain size for these studies ensured at least 5H and 15H spacing between the nearest building and the inlet and outlet patches, respectively. Here, H represents the building height. The height of the domain was up to 10H. For the sides of the simulation domain, the validation study used the side patches of about 10H. In the cube array simulations, the side patches were close to the buildings to simulate the effect of a continuously dense urban neighborhood [11]. For the top and side patches, studies used the slip boundary condition, which is a variation of the symmetry boundary condition.

To balance computational time with accuracy, this study used standard wall functions to describe the flow near building surfaces. The ground surface used atmospheric wall functions to simulate the surface roughness of common obstacles (0.3 m average roughness) [33]. Additional descriptions for the tradeoff of using wall functions for the outdoor CFD simulations are available in the literature [12,36]. OpenFOAM's snappyHexMesh tool generated a hexahedron-based unstructured mesh. Mesh cells farther from the building geometry were in the order of magnitude of the building height. SnappyHexMesh split refined cells nearer to the buildings up to six times. The use of Hexahedral cells allowed the aspect ratio to remain near 1 for most of the domain. To facilitate calculations of the near wall layer, SnappyHexMesh constructed thin layers with high aspect ratios parallel to the building surfaces to allow a y^+ ranging from 30 to 100.

At the simulation domain inlet, atmospheric boundary layer conditions defined the velocity and turbulent dissipation profiles [28]. Additionally, accurate modeling of the temperature field in the urban neighborhood required inlet temperature profiles. A previous validation case study, Liu et al. numerically calculated the temperature boundary layer by applying measured temperature data from the incoming airflow undisturbed by the neighborhood structures, and running the simulation for a large domain with a uniform temperature inlet [12,37]. Near the domain outlet, the needed temperature profile was available. This current validation study used the same approach to generate the inlet temperature profile. The current study uses an existing validation method defined as an indirect validation of the CFD simulations with the field temperature measurements in locations where measurements of the air velocities are impractical [12]. Furthermore, for the cube array simulations, the inlet temperature profiles also used the simulation approach tested and described in the literature [12,37]. To simulate these profiles, each neighborhood used a 550 m long

simulation domain, consisting of a long row of buildings to allow for the development of realistic flow conditions. At the inlet, a uniform temperature is prescribed, based on TMY3 (Typical Meteorological Year) weather data for the State College, PA location. The simulation converged to provide the temperature profiles following the last row of buildings, along with velocity, turbulent kinetic energy and turbulent dissipation profiles. The methodology outlined here is based on original recommendations from Takahashi [19]. The present study used weather data for every two hours from 8 a.m. to 6 p.m. for the design day (July 21).

The EnergyPlus simulations provided the temperature boundary conditions on the building surfaces. In addition, there was a heat flux occurring at the ground surface, driven by long-wave solar radiation, wind convection, and a constant temperature at "infinite" depth. In order to simplify the heat transfer interaction for the present study, a local scale empirical equation was used to estimate ground heat flux based on the objective hysteresis model [38]. All ground surfaces assumed coverage with grass to simplify the model as a reasonable assumption for the studied neighborhoods. The CFD study for Penn State campus neighborhood used the weather data from June 11, 2012 to define boundary conditions because the data collection took place during that day. The cube array neighborhood case study used two days, including the design day (July 21) and the worst-case scenario (July 19).

2.5. Grid convergence

A grid convergence study is carried out for the CFD simulations, following the GCI method [39]. The calculation of GCI is as follows:

$$GCI = \frac{F_s|\varepsilon|}{(r^p - 1)} \tag{13}$$

In this equation, F_s is the safety factor, set to 1.25, because it enabled a successful mesh refinement. Furthermore, ε is the percent error between the current mesh and the refined one. The variable r is the ratio of cell size between the two meshes, the refined and the original one. Finally, p is the order of convergence, calculated to be 1.7. The validation study used the fine grid with a GCI value of 4.5%. The cube array study used the medium grid because the fine grid showed only a 1.79% GCI value. Overall, the validation and cube array studies used 4.7 million and 5.2 million cells, respectively.

3. COP equations

Existing studies consider the degradation of the HVAC system performance due to the placement distance of the HVAC system components, the buoyancy effect inducted by heat rejection from condensers for high-rise buildings, and influence of the urban microclimate on efficiency of building cooling systems [22–26,40–43]. These studies show that it is expected to reach a 10 °C–13 °C temperature increase and ultimately 30% degradation in the performance of the cooling systems [24,40]. This study aims to assess degradation of the cooling systems due to the influence of the microclimate. The effect of urban density on the efficiency of cooling systems is due to the change in local temperatures that affect the COP of HVAC systems. Overall, the COP of a particular HVAC cooling system is a function of outdoor temperature and the system type. A few equations representing the COP based on outdoor temperature are available in the literature [22–26,40,41]; these are the COP equations used to quantify the process of COP degradation in this study. These equations usually assume the constant indoor temperature and regress the COP over a wide range of outdoor air temperatures. For example, Chow et al. [22] derived three COP equations for the indoor temperature values of 23 °C, 25 °C, and 27 °C, and the equations are valid for outdoor temperature within the range of 25 °C–45 °C. Most of the COP studies assumed 27 °C as the base indoor temperature. This study specially deals with COP, rather than Energy Efficiency Ratio (EER), which is a common air conditioning performance rating in the United States. The formulation of the two terms is equivalent, but the COP formulation is preferred due to its dimensionless definition.

This study categorizes the COP equations in four different types due to the inherent differences between these correlations. For different HVAC system, Table 1 shows the existing published COP equations grouped into the four types of equations. The first type of COP equations is empirical linear regressions based on manufacturer data. Similarly, the second type of COP equations uses second order regression equations to derive the COP equations. The third type of equations utilizes the manufacturer data to derive statistical correlations using non-linear inverse functions. The fourth type is the Carnot based equation. Since the Carnot efficiency defines the ideal system, for the actual HVAC systems, there is a need to modify the original Carnot equation. One of the most commonly used methods to modify the Carnot efficiency uses a correction coefficient. For example, one study used an exergetic efficiency coefficient g based on the Green Mark Platinum rating for buildings, which states that split HVAC units must achieve a COP of 3.34 at 35 °C outdoor dry bulb temperature [40]. Assuming a condensing temperature (T_1) of 2° above the off-coil temperature, and an evaporation temperature of 8 °C, the study calculates the coefficient g to be 0.321. Results using an unmodified Carnot COP calculation are not included in this study, as the COP would be unrealistically high. For example, the equation with the exergetic efficiency coefficient would result in a COP value more than three times larger than the value without the exergetic efficiency coefficient.

4. Actual urban neighborhood study

As a first step in the development of the proposed framework, this study conducted a validation of simulation results for an actual neighborhood. Specifically, OpenStudio and EnergyPlus software enabled modeling for the validation case study [44,45]. The studied campus dormitory buildings used the energy model inputs for the CBECS pre-1980's mid-rise apartment building (ASHRAE climate zone 5) from the Building Component Library (BCL) to specify the construction and schedules. Details of the construction and schedules are freely available through the U.S. Reference Buildings and the BCL repository [46,47]. For the validation CFD study, Fig. 3 shows the domain and building geometry. This study used the GCI presented in the research methodology to ensure the grid independency for the CFD simulations. The snappyHexMesh tool refined the mesh by changing the size of the cells in the background mesh, created in blockMesh. The background mesh, and, correspondingly, all of the cells in the mesh, are reduced by nearly 20 percent for the refined mash case. Fig. 4 shows the background mesh of both the baseline case and the refined case.

This study conducted validation of the CFD results for two turbulence models, RNG k-ε and Realizable k-ε. In addition, the temperature results are compared with the measured data for four different locations at three different elevations [37]. Due to local safety regulations, this study used wireless iButton sensors mounted to nearby telephone poles. The safety regulations and the need to install wireless sensors limited the use of the temperature sensors to iButton with accuracy of ±0.5 °C compared to the thermistors that have higher accuracy, usually ±0.1 °C. More details about the measurements, including the airflow and temperature

Table 1
Details of the HVAC COP equations used in this study.

Type	Equations	Description of variables	Correlation format	Source of data	HVAC system type
1	$COP = 4.825 - 0.0687T_o$ [24] (Valid for outdoor temperature between 25 °C and 45 °C and room temperature equals to 23 °C)	T_o is the outdoor air temperature	Linear regression	HVAC manufacture data	Split system
	$COP_R = 5.153 - 0.0738T_o$ [23] (Valid for outdoor temperature between 25 °C and 45 °C and room temperature equals to 25 °C)				Split system
	$COP = 5.241 - 0.0742T_o$ [22] (Valid for outdoor temperature between 25 °C and 45 °C and room temperature equals to 27 °C)				Split system
	$COP_{RTU} = 13.02 - 0.118T_o$[a] [41]			Onsite measurements	Packaged Rooftop Unit (RTU)
2	$COP = 12 - 0.35T_o + 0.0034T_o^2$ [26] (Valid for outdoor temperature between 21 °C and 39 °C and room temperature equals to 27 °C)	T_o is the outdoor air temperature	Second order regression	HVAC manufacture data	Split system
3	$COP = \frac{638.95 - 4.238T_o}{100 + 3.534T_o}$ [25] (Valid for room temperature equals to 27 °C)	T_o is the outdoor air temperature	Inverse	HVAC manufacture data	Split system
4	$COP = \frac{T_1}{T_2 - T_1}$	T_1 and T_2 are indoor and outdoor air temperatures	Carnot efficiency equation	Ideal efficiency of a cooling system	Any system
	$COP = g \times \frac{T_1}{T_2 - T_1}$ [40]	g is the exergetic efficiency coefficient	Modified Carnot equation	Onsite measurements	Split system

[a] T_o is outdoor temperature in Fahrenheit in this equation. Authors used scatter points in the figure to derive the COP equation.

variations, and the sensor installations are available in the literature [12,37]. Fig. 5 shows the locations of mounted sensors.

Table 2 shows the measured results for the urban thermal environment compared to the results from the CFD study for two different turbulence models. These results show that between the two models, the RNG k-ε model has better performance in simulating temperatures in the urban thermal environment, with 8 of the 12 temperature readings within the sensor margin of error, whereas the Realizable k-ε model has only 3 of the 12 readings within the sensor margin of error. Two of the values outside of the margin of error for the RNG k-ε model are only slightly outside of the 0.5 °C margin. The RNG k-ε model has the averaged absolute error of 0.4, while the Realizable k-ε averaged absolute error is 0.76. Overall, the Coefficient of Variation (CV) also for the two turbulence models show that the RNG k-ε model has a CV of 5.6%, while the Realizable k-ε model has a CV of 10.0%, suggesting that the RNG k-ε model is more suitable for this outdoor simulation. It is important to note that among different statistical tools, this study used CV as a statistical tool to assess differences between the simulation results and on-site measured data. In general, the CFD simulations slightly

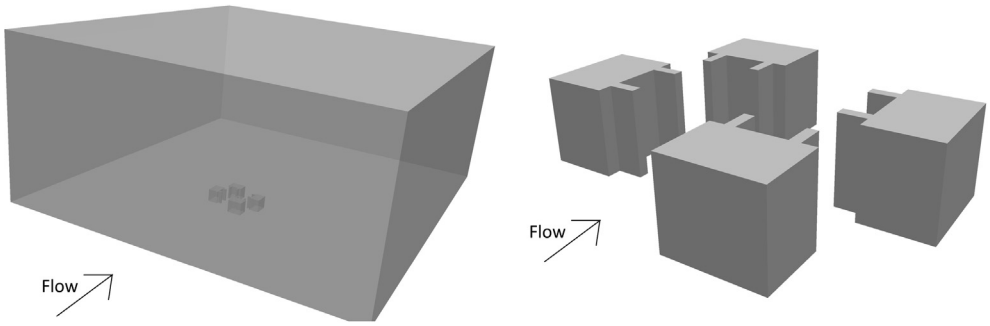

Fig. 3. CFD domain and building geometry for the validation case study.

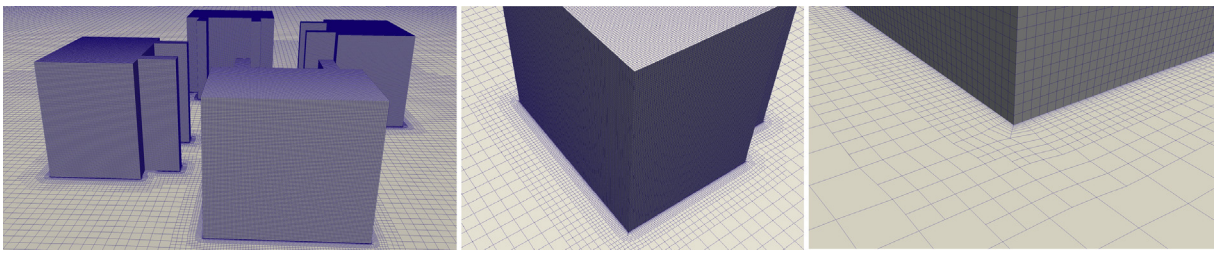

Fig. 4. Visualization of the fine mesh for the validation case study, showing the relative cell surface size for the building, near wall layers, and the surroundings.

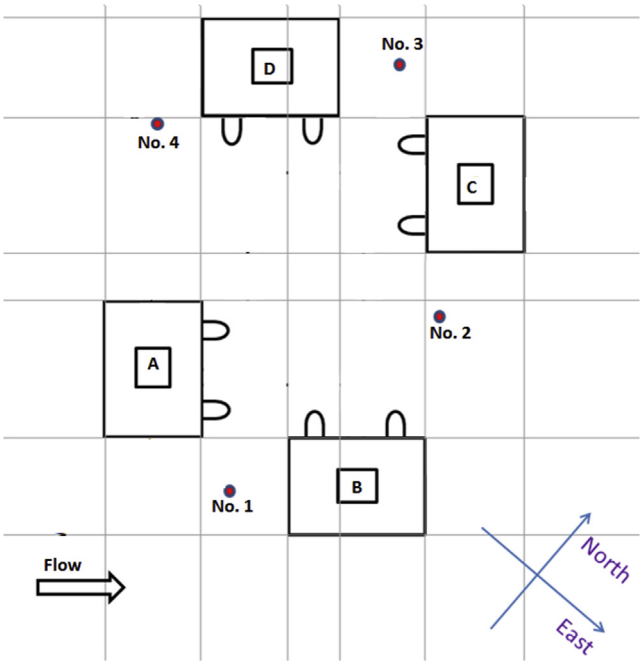

Fig. 5. Location of the sensors in the experimental measurements [12].

under predict the temperature compared to the field measurements, with the Realizable k-ε model predicting even lower temperatures.

A plot of turbulent thermal diffusivity (alphat) for the two simulations aids in understanding the reason for the discrepancies in temperature data from the different turbulence models, shown in Fig. 6. Specifically, Fig. 6 shows that the RNG k-ε simulation results in relatively lower turbulent thermal diffusivity flow than the flow with the Realizable k-ε simulation. The figure presents the alphat variable at 10 m elevation starting at the inlet and ending just before the buildings. The Realizable k-ε model predicts a larger alphat at the inlet, and the alphat variable decays slightly less through the domain. This plot indicates that the Realizable k-ε model may be over predicting the turbulent kinetic energy used to calculate the turbulent viscosity and turbulent thermal diffusivity.

Furthermore, Fig. 7 presents the incoming temperature profile preceding the buildings. From Fig. 7, it is clear that the temperatures in the RNG k-ε case are higher until around 60m elevation, at which and the temperatures from the Realizable k-ε model

Table 2
Temperature data from CFD compared to measurement.

Location	Height (m)	Temperature from realizable k-ε model (°C)	Temperature from RNG k-ε model (°C)	Temperature from onsite measurements (±0.5 °C)
1	2	28.9	29.3	29.1
	4	28.8	29.2	29.6
	6	28.7	29.2	29.2
2	2	29.1	29.5	29.7
	4	29.0	29.4	29.8
	6	28.9	29.4	30.2
3	2	28.8	29.3	30.2
	4	28.8	29.2	29.8
	6	28.8	29.2	29.3
4	2	29.0	29.4	29.9
	4	29.0	29.4	29.2
	6	28.9	29.4	29.9

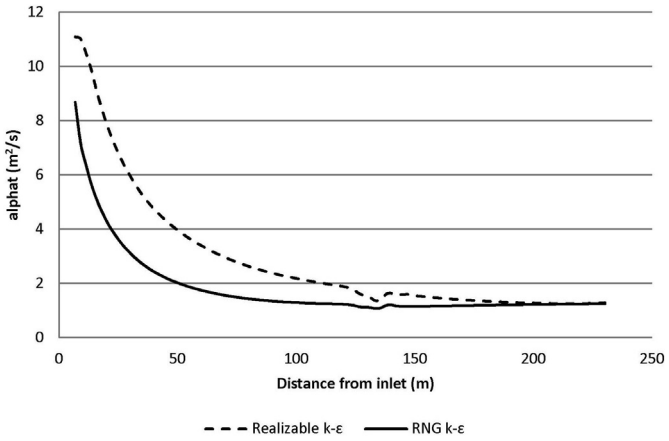

Fig. 6. Freestream decay of turbulent thermal diffusivity (alphat) from the inlet to the buildings.

becomes larger. Both cases apply the same temperature boundary layer at the inlet of the simulation domain, so the Realizable k-ε model is causing the temperatures in the domain to diffuse faster from the original specified boundary layer. Fig. 8 illustrates that the turbulent thermal diffusivity is larger in the Realizable k-ε case near the buildings.

The results of this study show that OpenFOAM combined with EnergyPlus and local weather data for boundary conditions can be a reasonably accurate method to calculate the local temperatures and microclimate in urban areas. The study also revealed that the RNG k-ε model has closer agreement with the measured temperature data from the actual urban environment compared to the Realizable k-ε model.

5. Study of urban neighborhood densities

This study builds upon the developed framework and findings from the validation case study to quantify the impacts of different urban neighborhood densities on the COP of the HVAC systems. Similar to the validation study, this study uses OpenStudio and the SketchUP plugin to create the energy model for the building of interest and derive the distribution of the exterior building surface temperatures for the airflow simulations. The model represents a three-story building with 10 × 10 × 10 m volume divided into a core zone and four perimeter thermal zones. To enable a comparative analysis with the actual building, the energy model uses the CBECS pre-1980's building material for the building envelope with a fixed WWR of 0.25. Shading blocks, representing neighboring buildings, simulate the solar environment for each urban density neighborhood.

The CFD case setup follows the same procedures as the one previously used for the validation study. The inlet boundary uses profiles for the flow variables k, ε, velocity, and temperature. The sides of the domain apply a symmetry condition, simulating the effect of neighboring buildings evenly spaced and extending indefinitely, representing a large urban area. The distance from the side buildings to the symmetry wall is half of the distance of the building spacing, assuming that the selected buildings are located in an infinite array of buildings extending perpendicular to the wind direction. The study takes place over a ten-hour period with simulations taking place every two hours, from 8:00 to 18:00 h. The wind speed is approximately 5 m/s at an elevation of 10 m, but the actual speeds vary slightly for the different urban densities, giving an approximate Reynolds number of $Re = 3.2 \times 10^6$. This study uses the grid refinement approach similar to the actual urban

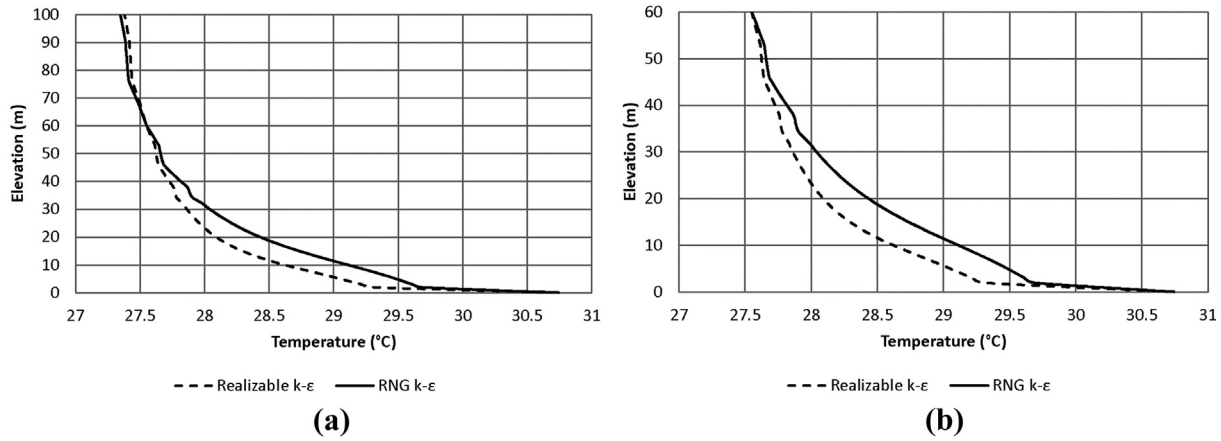

Fig. 7. The temperature profile directly preceding the buildings in the validation case study for: (a) 0–100 m elevation and (b) 0–60 m elevation.

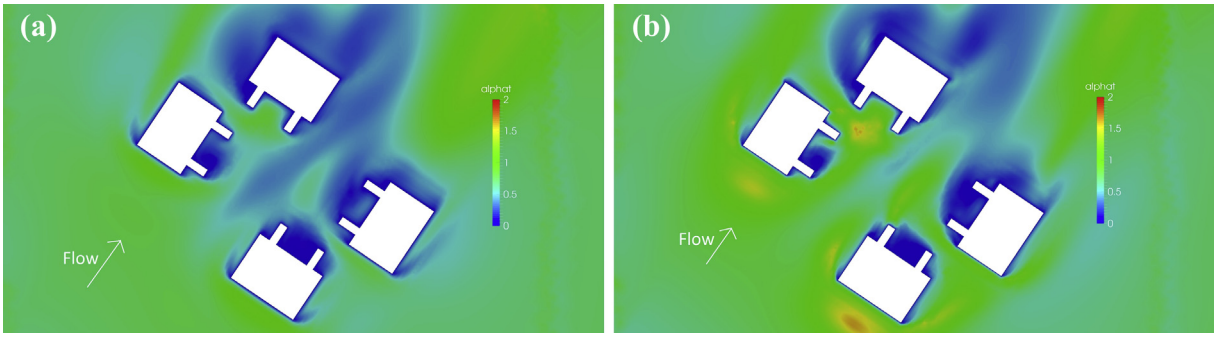

Fig. 8. Alphat plot for (a) RNG k-ε and (b) Realizable k-ε simulations.

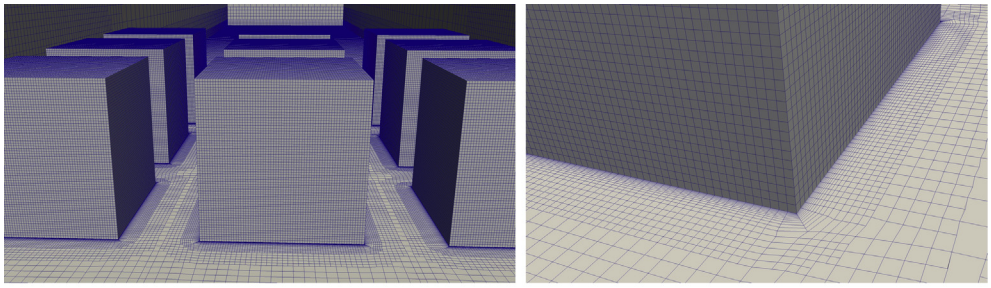

Fig. 9. Medium computational mesh for 0.44 case study: (a) Overall mesh of the domain and (b) Near wall mesh.

neighborhood study to conduct the grid independency evaluation. Fig. 9 displays the computational mesh used for the 0.44 density case. The medium mesh was refined by a ratio of 1.25 to get the fine mesh. The calculated relative error was 0.67 percent. For a second order level of convergence, the refinement study results in a grid convergence index of 1.79, deeming the medium refinement mesh sufficiently refined. Fig. 10 illustrates the airflow simulation results for the refined mesh featuring recirculation eddies between the densely placed buildings.

6. COP for different urban neighborhood densities

The COP calculations use the results of the temperature distributions to quantify the influence of the urban neighborhood on the performance degradation of the building cooling systems.

6.1. Selection of study days

To assess the degradation of the COP for cooling HVAC systems, it is important to select representative days for the CFD simulations to inform the model boundary conditions. Building HVAC designers typically use the summer design day, July 21, to design the cooling systems. Therefore, this study selects the summer design day as one of the days for the urban density study. In addition to the selection of the design day, an additional summer day can provide further insight. Based on the results of the literature review, solar radiation is one of the primary contributors to the variation of the local air temperature for buildings located in urban neighborhoods. The present study used the daily average from 8:00 to 18:00 h, and the day with the highest product of solar radiation; the air temperature with the maximum value is July 19. By selecting this day for the

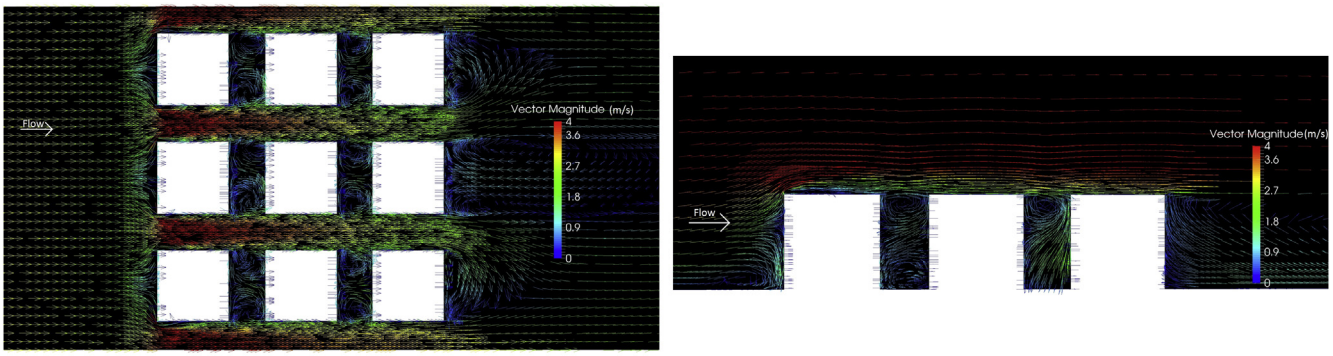

Fig. 10. Airflow around the buildings for the urban neighborhood study: (a) Top view and (b) Centerline vertical view.

analysis, this study considers the maximum variation of the local air temperature due to the urban neighborhood density and driven by the weather conditions from a hot day, and a high amount of solar radiation for the University Park, PA. This combination mimics the methodology used in the calculation of sol-air temperature to incorporate the influence of the solar radiation in the analyses. To find the day with the highest solar radiation, this study summed and averaged the direct and diffuse over 24 h periods. Similarly, this study calculated the daily averages of the air temperature. Finally, the yearly max product of daily averaged air temperatures and solar radiation provided the extreme weather day selected for the study. The following equation summarizes the criteria to define the extreme weather day for this study.

$$Selected\_Day = \max\left(\frac{\sum_{i}^{n}(T_o \times (Direct\ Solar\ Radiation + Diffuse\ Solar\ Radiation))_n}{n}\right) \quad (14)$$

where T_o is the outdoor environmental temperature, and n is the number of data points equal to the number of hours in a year. It is important to note that days in June often have high solar radiation, but a lag caused by the thermal mass of the earth keeps air temperatures relatively cool. The methodology used to select this particular day of study is similar to the process of selecting days for HVAC peak load calculations. This process was employed due to the additional potential implications that this study may provide for such peak load calculations. Fig. 11 shows the daily averaged solar radiation for both July 19 and 21. These results suggest that July 21 has clouds blocking most of the solar radiation right around the solar maximum (noon). Furthermore, July 19 is more consistently sunny. These differences allow an opportunity to witness the effect of sudden shading on the neighborhood local temperatures.

This study extracted centerline air temperatures along the windward walls and leeward walls from the CFD simulations to determine the effectiveness of the on-coil temperature for the COP of window type cooling systems. Fig. 12 plots the temperature of the windward and leeward surfaces for the 0.04 and 0.4 plan area densities on July19 and July 21. Fig. 12(a) shows that the windward temperatures in the 0.44 case study are consistently higher than temperatures in all of the other locations. The 0.44 leeward case study results in temperatures similar to the temperature of the 0.04 leeward case study. Furthermore, the temperatures for the 0.04 windward case study are the lowest. The temperatures also follow a parabolic profile, with a peak at about 14:00 h Fig. 11 shows that maximum solar radiation occurs at 12:00 h. There appears to be around a two-hour lag between maximum solar radiation and maximum air temperature. The windward and leeward profiles for July 21 depicted in Fig. 12(b) illustrate a different temperature variation compared to the temperature variation on July 19. The results show that the solar radiation plays an important role in determining the variation of the temperatures for the windward and leeward walls. Similar to July 19, the windward airflow simulations for the densest urban configuration result in the highest temperature values, and the simulations of the leeward walls for the least dense case study result in the lowest temperature values.

For a better understanding of the windward and leeward temperature values, Fig. 13 displays the temperature contours around buildings for both 0.44 and 0.4 plan area densities. The middle building is the one used to examine local temperatures. The leeward sides of the buildings are the first to experience sunlight

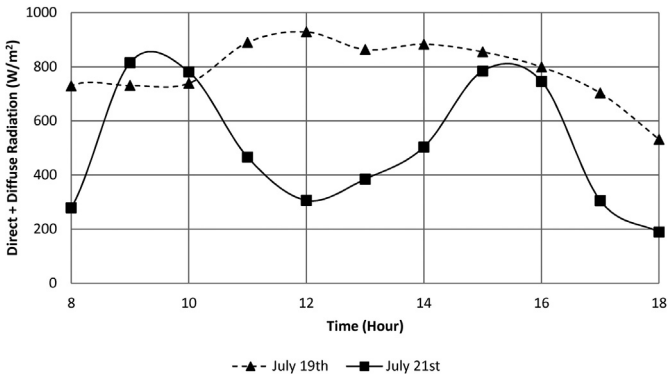

Fig. 11. Hourly solar radiation for the July 19 and July 21 selected study days.

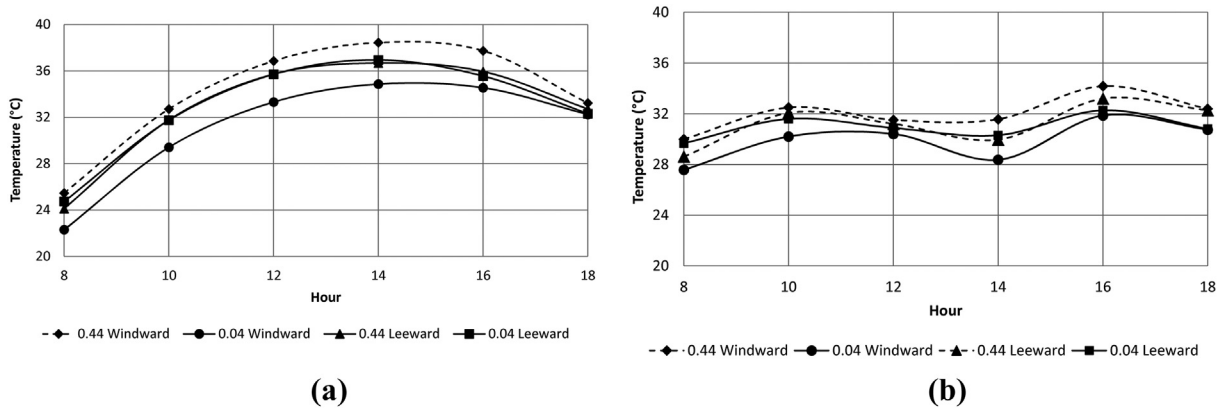

Fig. 12. Average windward and leeward air temperatures for the smallest and largest density neighborhoods measured at each simulated hour (a) July 19 (highest solar radiation and air temperatures) and (b) July 21 (Design day).

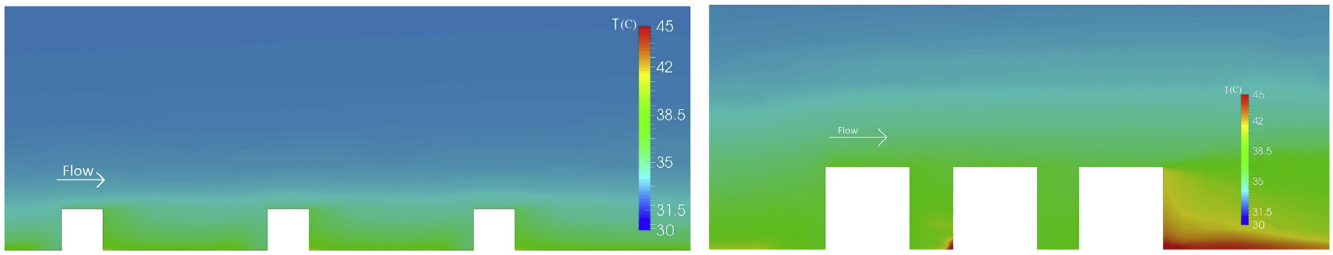

Fig. 13. Temperature contours for highest and lowest density cases, July 19, 14:00 h.

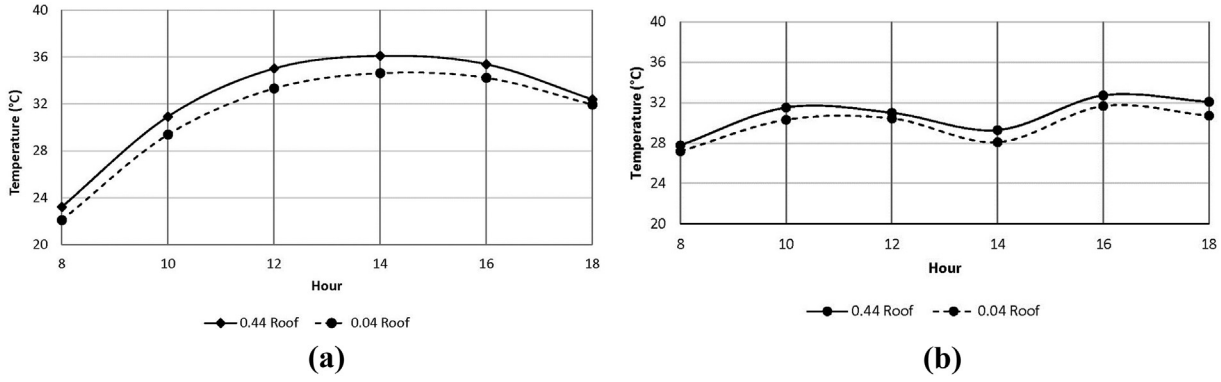

Fig. 14. Rooftop air temperatures for (a) July 19 and (b) July 21.

because they face east. This orientation creates a building temperature wake energized by the heat stored in the building walls from the beginning of the day. In the 0.44 case study, a representative building is located close to the neighboring upwind building, putting the representative building much closer to the upwind building's wake and the elevated temperatures resulting from it. This also explains how the leeward side in the 0.04 case is consistently warmer than its windward side, since the leeward side is in the building's own temperature wake.

Fig. 14 shows the rooftop temperatures for the two selected days. Similar to the windward and leeward temperatures, the rooftop temperature peak lags the solar radiation peak by about two hours on July 19. The 0.44 case has higher temperatures for both days. This is due to the inlet temperature profile that has much higher temperatures above 10 m elevation due to the skimming flow, resulting in the air above the roof not mixing with the air below. The results for the design days show similar temperature variations for the windward and leeward walls.

6.2. Local temperature effect on COP

This study calculates COP as a function of local temperatures of the air near the windward, leeward, and rooftop sides for the building of interest. The results show the variation of the normalized COP for the most dense case ($\lambda_p = 0.44$) and the least dense case ($\lambda_p = 0.04$) during the two days of July 19 and July 21. These results provide COPs for the windward walls, leeward walls, and the roofs. The two extreme urban plan area densities illustrate the degradation in COP of cooling systems due to increased temperatures in the denser urban environment. Therefore, this study provides a figure for each day representing the windward walls, leeward walls, illustrating normalized COP as a ratio of the densest

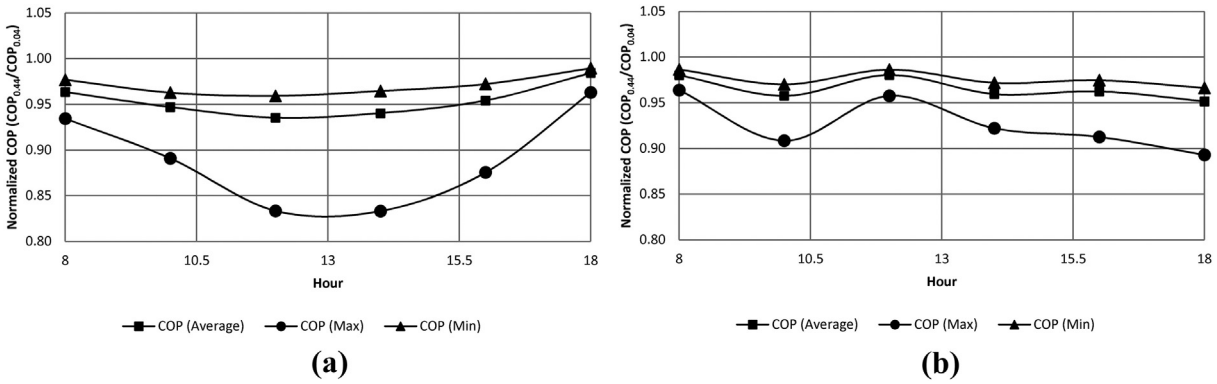

Fig. 15. Variation of the normalized COP ($COP_{0.44}/COP_{0.04}$) for cooling systems installed on the roof for (a) July 19 and (b) July 21.

case ($\lambda_p = 0.44$) to the least dense case ($\lambda_p = 0.04$), defined as $COP_{0.44}/COP_{0.04}$. For each of the configurations, the figures include averaged, minimum, and maximum variations of the normalized COP. Normalized COP is defined to include all of the equations in the analyses and make the results independent of the COP equations. In addition, the selection of the normalized COP allows presenting the most representative figures. While the averaged values represent the average values of COP based on all of the selected COP equations, the maximum and minimum values show the extreme variation of the COP values.

Fig. 15 illustrates the performance of the cooling systems installed on the roof based on the temperature values for the centerline on the roof. In general, all of the COP equations for the dense case have lower values compared to the COP values for the least dense case. For both of the selected days, the variation of the normalized COP for the minimum and averaged values follow a similar trend, suggesting that majority of the COP equations perform similarly. Among the used COP equations, variation of the normalized COP for the NBI's equation is different from other equations due to its inherent difference [41]. On July 19, the COP has the maximum value during the morning at 8:00 h and decreases to the lower value at 13:00 h. Then, after 13:00 h, the COP increases until 18:00 h. The variation of the COP values for July 21 does not follow a specific trend due to the sudden variation of the solar radiation illustrated in Fig. 14. The maximum COP degradation is about 17% reduction occurring at 14:00 h for July 19, and 11% for July 21 occurring at 18:00 h. The minimum COP degradation resulting from the study is 1% for both of July 19 and 21. The average COP reduction for the different COP equations is approximately 4% for July 19 and 3.5% for July 21. Overall, the roof warming contributes to this COP degradation because the higher temperature wake of the previous building diffuses upwind above the roof of the building of interest. Additional warming is due to the higher inlet temperature conditions in the $\lambda_p = 0.44$ case because the denser neighborhood resulted in a higher temperature thermal boundary layer. When the solar radiation is stronger, the solar radiation attributes to the higher incoming heat flux to the urban neighborhood, higher storage of heat flux, and ultimately higher air temperature.

The results for the windward walls show that the windward walls are highly affected by the characteristics of the urban neighborhood. The COP values for the installed cooling systems on the windward walls for the case of plan area density of 0.44 have lower values compared to the windward COP for the case of 0.04 or even the COP for the rooftop systems. Fig. 16 illustrates the ratio of the normalized COP ($COP_{0.44}/COP_{0.04}$) for the windward walls. Fig. 16(a) shows the COP results for July 19, and Fig. 16(b) illustrates the COP results for July 21. The NBI equation [41] is removed from the analysis since it is specifically developed for the rooftop units (RTUs). The maximum COP reduction is approximately 16% and 13% for July 19 and July 21, respectively. In addition, the average COP reduction is 8.2%, and 7.4% for July 19 and July 21, respectively. Furthermore, 2.4% and 2.1% are the minimum COP reductions for July 19 and July 21, respectively. Overall, a comparison between the variation of the minimum, maximum, and averaged normalized COP values show that the normalized COP values follow a similar

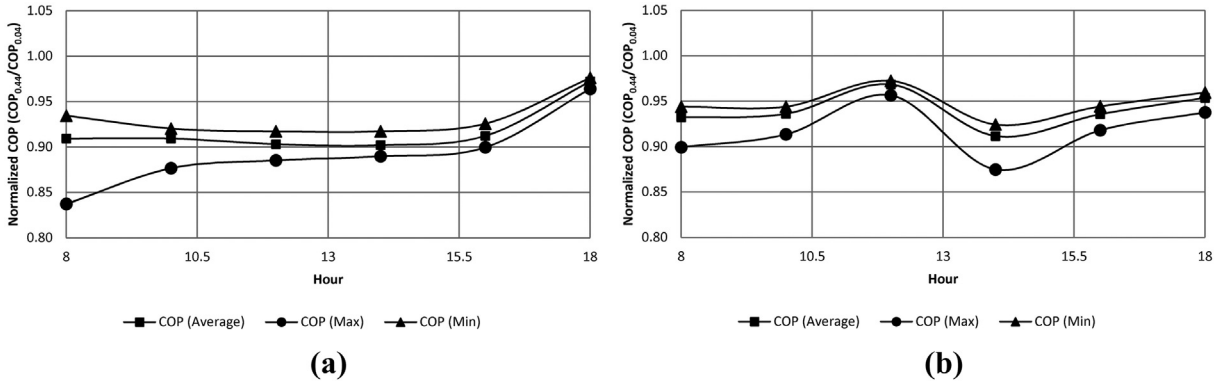

Fig. 16. Variation of normalized COP ($COP_{0.44}/COP_{0.04}$) for cooling systems installed on the windward walls for (a) July 19 and (b) July 21.

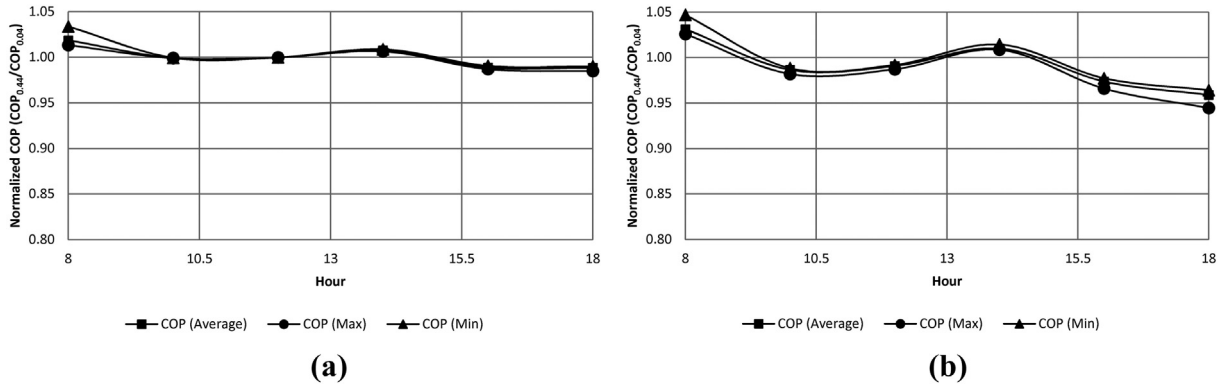

Fig. 17. Variation of normalized COP ($COP_{0.44}/COP_{0.04}$) for cooling systems installed on the leeward walls for (a) July 19 and (b) July 21.

pattern with the exception of 8:00 to 10:00 h in the morning on July 19. This pattern occurs due to the maximum variation of the temperature from 8:00 to 10:00 h illustrated in Fig. 14.

A comparison between the normalized COP variations for the leeward walls with the windward walls and roofs indicates the normalized COP for the leeward walls have lower variations. Fig. 17(a) and Fig. 17(b) show that the variation of the averaged, maximum, and minimum normalized COP values are very close for the leeward walls, suggesting that all of the equations estimate similar variations with the urban density changes. The maximum COP reduction for the case on July 19 is approximately −3%, and for the case on July 21 is approximately −5%. In summary, the COP degradation for the leeward walls for both July 19 and 21 does not vary significantly through the day. The average COP degradation is 0.0% and 1.1% for July 19 and July 21, respectively. Overall, the leeward sides of the building do not show a clear trend, with both increases and decreases in COP due to density depending on the time of day. The upwind neighboring building's wake influences the temperatures at the windward side of the building of interest. In the $\lambda_p = 0.44$ case, the upwind building's thermal wake has a much more profound influence on the incoming air temperature than the thermal wake in the $\lambda_p = 0.04$ case because the building of interest is much closer to the upwind building in the $\lambda_p = 0.44$ case. The leeward cases show no clear trend because the COP calculations use temperature data directly in front of the building of interest. Therefore, the influence of thermal wake of the upwind neighboring building is approximately equal in both the 0.44 and 0.04 cases.

Fig. 18 summarizes the results of the temperature and COP variations for the six selected urban plan area densities on July 19 at 14:00 h. This figure represents COP results for the simultaneous maximum air temperature and incoming solar radiation. Fig. 18(a) shows the temperature variations for windward walls, leeward walls, and roofs. The figure represents the temperature and normalized COP data at 0.5 m from the building surface at the centerline of the building. Furthermore, this study samples the leeward and windward data from 0 m to 10 m elevation, and the roof data on the centerline extending in the direction of incoming airflow. The urban neighborhood influences the temperature values for the windward walls, while the temperature values for the leeward walls show the least variation. The temperature values for the roof gradually increase with the increase of the urban plan area density. Fig. 18(b) illustrates the COP variation with urban plan area density for the windward, leeward, and roof of the building using averaged normalized COP values defined as the COP of the building in the selected urban neighborhood divided by the baseline COP represented with $COP_{0.04}$. The results confirm that the COP of roofs and windward walls are sensitive to the urban plan area density, while the leeward side compared to the windward walls and roofs has the least variation. The absolute reductions of the COP for the windward walls and roofs are 10% and 7%, respectively. It is important to note that this study uses the average of the reviewed equations to derive the normalized COP values. The results of a sensitivity analysis show that the overall standard deviation for the windward walls, leeward walls, and roofs are 0.01, 0.00, and

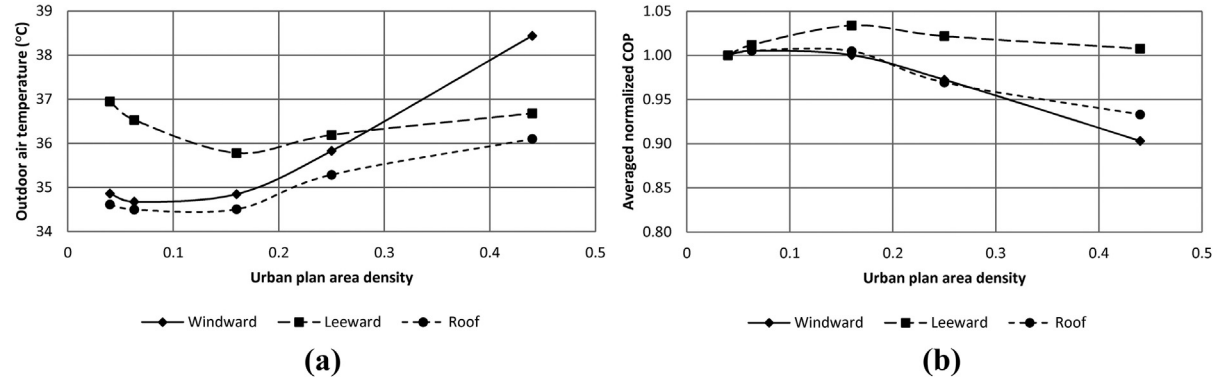

Fig. 18. Temperature and COP variations for windward, leeward, and roof with the urban plan area density for the peak time (14:00 h on July 19): (a) Temperature and (b) COP variations.

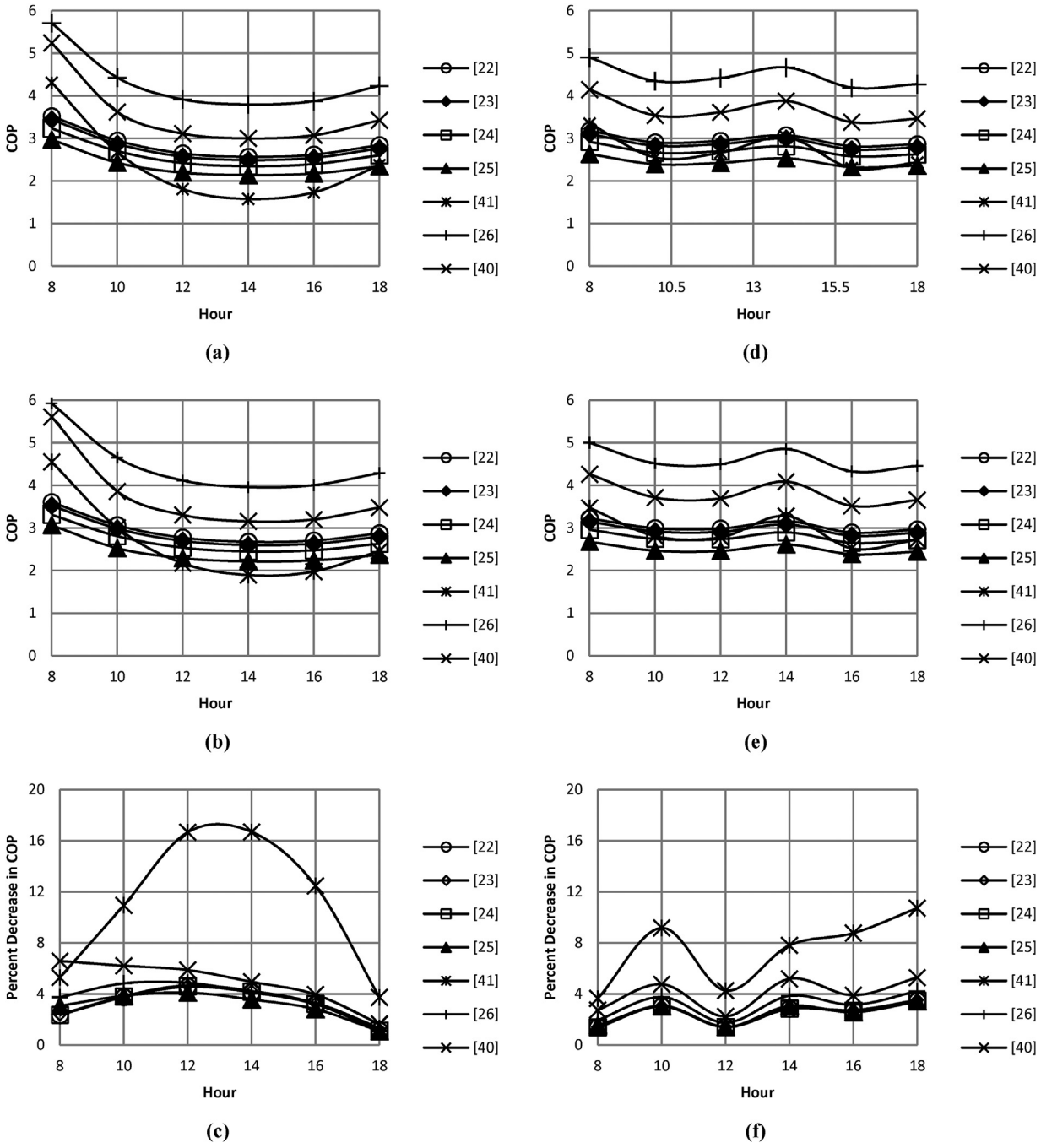

Fig. 19. COP of cooling systems and COP degradation when the plan area density of the urban neighborhood is 0.44 and 0.04 for cooling systems installed on the roof depicted in Figures (a) to (c) for July 19th and illustrated in Figures (d) to (f) July 21st. (a) COP variation for 0.44, (b) COP variation for 0.04, (c) Percent decrease in COP from 0.04 to 0.44, (d) COP variation for 0.44, (e) COP variation for 0.04, and (f) Percent decrease in COP from 0.04 to 0.44. Numbers in the legend represent the COP equation used based on the reference numbers in the Reference section.

0.01,respectively, suggesting that for this specific configuration all of the equations have a similar response.

7. Discussions

7.1. Performance of COP correlations

To provide performance of different COP correlation used in this study, this discussion presents an example of the calculations for the rooftop units. Fig. 19 illustrates the performance of the cooling systems installed on the roof based on the temperature readings for the centerline on the roof. In general, all of the COP equations for the dense case depicted in Fig. 19(a) and (b) have lower values compared to the least dense case values illustrated in Fig. 19(d) and (e). In addition, for both of the urban neighborhoods, the COP has the maximum reading during the morning at 8:00 h and decreases to the lower value at 14:00 h. Then, after 14:00 h, the COP increases until 18:00 h. Fig. 19(c) and (f) depict the differences between the COPs for the selected two urban plan area densities. Among the used COP equations, NBI equation [41], Ryu equation [26], and Bruelisauer equation [40] perform slightly different than the other equations due to their inherent differences while the other

equations perform similarly. In addition, it is important to note that the most relevant equation for the roof analysis is the NBI equation since the experiments used to develop this equation involved the use of RTUs. The maximum COP degradation for NBI's equation predicts a 16.7% reduction occurring at 14:00 h for July 19th and 10.7% for July 21st. The minimum degradation resulting is 1.1% and 1.4% for July 19th and 21st, respectively. The average COP reduction for the different COP equations are 4% for July 19th and 3.5% for July 21st. Overall, the roof warming is related to this observation as well, because the higher temperature wake of the previous building is diffused upwards above the roof of the building of interest. Additional warming is due to the higher temperature initial conditions in the $\lambda_p = 0.44$ case, because the denser collection of buildings resulted in a higher temperature thermal boundary layer. When the solar radiation is stronger, the COP values are higher, and the COP is less sensible to the outdoor air temperature.

7.2. Placement of HVAC systems

Placement of the HVAC systems is one of the important parameters in the design and retrofit of buildings. Depending on the type of the building and location of the building, designers rely on common design practices. Larger commercial buildings typically use rooftop HVAC equipment, which minimizes issues regarding structural, esthetic, and ventilation distribution. Certain regions, as outlined by Chow [23,24], Choi [25], and Brueslisauer [40], commonly place HVAC system condensing units in a much more distributed pattern, especially in regions where split type systems are popular. Distributed systems provide certain advantages that resulted in continued usage in certain areas. Multiple packaged units serving a building reduce the number of zones conditioned by each unit. When the units serve fewer zones, the potential to reduce, or eliminate energy use from reheat coils becomes much more viable. The results of the current study support further study into placement of the HVAC systems in different locations of the building.

One of the main implications of the results of this study could be the support for placement of secondary HVAC systems (more common in fast developing countries) in addition to the common (in the United States) centralized rooftop mounted HVAC systems for large commercial buildings. The results of this study showed that when the buildings are close to each other, the leeward surface of the building has a lower degradation in the efficiency of the cooling systems. Therefore, this study recommends installing the secondary packaged systems on the leeward façade of the building according to the prevailing wind directions. In low-density neighborhoods, it is clear that HVAC systems on the leeward and windward sides of buildings will experience a lower COP degradation as these systems are farther from existing building wakes.

Overall, this study showed that for the considered weather/flow conditions and this particular urban geometry, there could be up to 17% reduction in the performance of the cooling systems due to the influence of the local microclimate. An addition of 17% to the degradation estimated by the existing studies that quantified the influence of the condensing unit placement could result in a nearly 40% reduction of the cooling system COP. Therefore, there is a need to consider placement of the HVAC systems and influence of the microclimate on the degradation of cooling system performance for the HVAC system design and installation.

7.3. Closing remarks

This study aimed to construct a methodology for conducting urban scale CFD simulations using free and open source software packages. As the software tools are improved, and computational power increases, similar studies can increase the accuracy and complexity of simulations covered in the present study. Coupling of the calculation of surface-to-surface radiation transfer in both the building energy and CFD simulations would further improve the accuracy of the results. The addition of such a calculation is the logical next step for the methodology/tools used in this study.

The present study considered the peak conditions for the degradation of HVAC operational COP. A follow up study could cover variation of the operational COP for each month to quantify the influence of urban density on seasonal performance and develop Seasonal Energy Efficiency Ratio (SEER). In addition, for the readers those are more familiar EER, the COP and EER are directly proportional to each other since COP is equal to EER/3.412; therefore, they are interchangeable. COP is favored due to its non-dimensional representation of efficiency, whereas EER requires conversion of units. The present study is limited to one flow orientation in a single climate. To develop a more comprehensive relationship between urban density and COP, automation and high computing power provide a potential to study a wide range of climates, neighborhood shapes, and flow conditions. Such a study could prove immensely useful for urban planning and campus design.

Another important note is that while in the U.S., rooftop units are commonly used, in the Asian countries the window units are commonly used [22,23,26]. Therefore, based on the location of the building, there is a need to consider different installation location of the HVAC systems, including roofs, windward walls, and leeward walls. In addition, future studies focusing on the design of the urban neighborhoods could consider the heat rejection of the HVAC systems. Since consideration of the HVAC system location requires a sensitivity study to find the optimal place of the HVAC systems, this study does not consider it in the simulations.

This study relied on the few COP correlations published in peer reviewed journal publications that quantify the rate COP based on the outdoor air temperature. One of the aims of this paper was to build upon the existing COP correlations. A potential area for the future studies is to develop more robust COP curves and consider additional factors in predicting HVAC performance based on part-load or local humidity ratio.

8. Conclusions

This study quantified the effect of urban neighborhood on the performance of building cooling systems and developed a procedure to calculate the local air temperatures using airflow CFD simulations and building surface temperatures from building energy simulations. OpenFOAM and EnergyPlus provided the CFD and building energy simulations, respectively, and enabled reliance on open source simulation engines. This study used this analysis framework for an actual urban neighborhood to validate the air temperature values with on-site measured data. The results of this validation showed that the consideration of thermal boundary conditions on building surfaces is important. Turbulence modeling also affected the thermal boundary layer with the Realizable k-ε model decreasing calculated temperatures by 0.4 °C compared to the RNG k-ε model predictions due to over prediction of turbulent thermal diffusivity. RNG k-ε showed a better agreement with the on-site data resulting in a Coefficient of Variation (CV) of 5.6% compared to the Realizable k-ε turbulence model that resulted in a CV of 10.0%.

After the validation, this study used the developed framework for the urban density study to derive the airflow temperatures for the quantification of COP degradation. This study provided a critical literature review to categorize the existing COP equations into four categories based on type of the function to predict the variation of the COP based on the outdoor air temperature. Interestingly, all of the reviewed equations provided similar relative differences when

calculating COP values with the exception of NIB equation, specifically developed for rooftop units. Furthermore, to evaluate the degradation on the COP values, the results directly compared a normalized COP representing $COP_{0.44}/COP_{0.04}$ for the dense case, plan area density of 0.44, to the least dense case, plan area density of 0.04 as. The results for the present study's climate and flow conditions suggested that the COP values of rooftop and windward/window HVAC systems decreased by up to 16% and 17%, respectively. The results of this study support quantification of different HVAC system installations, including rooftop installation mostly found in the U.S. and the window unit installation mostly found in Asian countries. Overall, the study executed the co-simulation of airflow and building energy models to calculate urban thermal environments and proposed preferred locations for the primary and secondary HVAC systems. When the buildings are close to each other similar to common configuration of urban neighborhoods in the urban areas, the leeward side of the buildings is the preferred location for the installation of the HVAC systems. When the buildings are far from each other, the leeward and the windward sides of the buildings are both preferred location for the installation of HVAC systems.

Acknowledgments

This study was sponsored by the EFRI-1038264/EFRI-1452045 award from the Division of Emerging Frontiers in Research and Innovation (EFRI), National Science Foundation (NSF). Authors would like to thank Mostapha Sadeghipour Roudsari and Kai Liu for their technical support during the preparation of this work.

References

[1] Cohen B. Urbanization in developing countries: current trends, future projections, and key challenges for sustainability. Technol Soc 2006;28(1–2):63–80.
[2] Urban Heat Island Basics. United State Environmental Protection Agency.
[3] M. Santamouris, C. Cartalis, A. Synnefa, D. Kolokotsa, On the impact of urban heat island and global warming on the power demand and electricity consumption of buildings–a review, Energy Buildings.
[4] Kolokotroni M, Giannitsaris I, Watkins R. The effect of the London urban heat island on building summer cooling demand and night ventilation strategies. Sol Energy 2006;80(4):383–92.
[5] Santamouris M. On the energy impact of urban heat island and global warming on buildings. Energ Build 2014;82(0):100–13.
[6] Allegrini J, Kämpf J, Dorer V, Carmeliet J. Modelling the urban microclimate and its influence on building energy demands of an urban neighbourhood. CISBAT 2013, Lausanne, Switzerland. 2013.
[7] Alexandri E, Jones P. Temperature decreases in an urban canyon due to green walls and green roofs in diverse climates. Build Environ 2008;43(4):480–93.
[8] Chen H, Ooka R, Huang H, Tsuchiya T. Study on mitigation measures for outdoor thermal environment on present urban blocks in Tokyo using coupled simulation. Build Environ 2009;44(11):2290–9.
[9] Hang J, Luo Z, Sandberg M, Gong J. Natural ventilation assessment in typical open and semi-open urban environments under various wind directions. Build Environ 2013;70(0):318–33.
[10] Allegrini J, Dorer V, Carmeliet J. Analysis of convective heat transfer at building façades in street canyons and its influence on the predictions of space cooling demand in buildings. J Wind Eng Ind Aerodyn 2012;104–106(0):464–73.
[11] Liu J, Srebric J, Yu N. Numerical simulation of convective heat transfer coefficients at the external surfaces of building arrays immersed in a turbulent boundary layer. Int J Heat Mass Transf 2013;61:209–25.
[12] Liu J, Heidarinejad M, Gracik S, Srebric J, Yu N. An indirect validation of convective heat transfer coefficients (CHTCs) for external building surfaces in an actual urban environment. Build Simul 2015:1–16.
[13] Saneinejad S, Moonen P, Carmeliet J. Coupled CFD, radiation and porous media model for evaluating the micro-climate in an urban environment. J Wind Eng Ind Aerodyn 2014;128(0):1–11.
[14] Evins R, Dorer V, Carmeliet J. Simulating external longwave radiation exchange for buildings. Energ Build 2014;75(0):472–82.
[15] Perez KX, Cole WJ, Rhodes JD, Ondeck A, Webber M, Baldea M, et al. Nonintrusive disaggregation of residential air-conditioning loads from sub-hourly smart meter data. Energ Build 2014;81(0):316–25.
[16] Kim M, Payne WV, Domanski PA, Yoon SH, Hermes CJL. Performance of a residential heat pump operating in the cooling mode with single faults imposed. Appl Therm Eng 2009;29(4):770–8.
[17] Ashie Y, Thanh Ca V, Asaeda T. Building canopy model for the analysis of urban climate. J Wind Eng Ind Aerodyn 1999;81(1–3):237–48.
[18] Mirzaei PA, Haghighat F. Approaches to study urban heat island – abilities and limitations. Build Environ 2010;45(10):2192–201.
[19] Takahashi K, Yoshida H, Tanaka Y, Aotake N, Wang F. Measurement of thermal environment in Kyoto city and its prediction by CFD simulation. Energ Build 2004;36(8):771–9.
[20] Huang H, Ooka R, Kato S. Urban thermal environment measurements and numerical simulation for an actual complex urban area covering a large district heating and cooling system in summer. Atmos Environ 2005;39(34):6362–75.
[21] Mochida A, Lun IYF. Prediction of wind environment and thermal comfort at pedestrian level in urban area. J Wind Eng Ind Aerodyn 2008;96(10–11):1498–527.
[22] Chow TT, Lin Z, Wang QW, Lu JWZ. Studying thermal performance of split-type air-conditioners at building re-entrant via computer simulation. In: Proceedings of building simulation 1999, Kyoto, Japan; 1999.
[23] Chow TT, Lin Z, Wang QW. Effect of building re-entrant shape on performance of air-cooled condensing units. Energ Build 2000;32(2):143–52.
[24] Chow TT, Lin Z, Yang XY. Placement of condensing units of split-type air-conditioners at low-rise residences. Appl Therm Eng 2002;22(13):1431–44.
[25] Choi S-H, Lee K-S, Kim B-S. Effects of stacked condensers in a high-rise apartment building. Energy 2005;30(7):968–81.
[26] Ryu K, Lee K-S, Kim B-S. Optimum placement of top discharge outdoor unit installed near a wall. Energ Build 2013;59(0):228–35.
[27] Franke J, Hellsten A, Schlünzen H, Carissimo B. Best practice guideline for the CFD simulation of flows in the urban environment. COST 2007.
[28] Gracik S. The effect of urban density on building HVAC performance. Mechanical Engineering, The Pennsylvania State University; 2014.
[29] Liu J, Heidarinejad M, Gracik S, Srebric J. The impact of exterior surface convective heat transfer coefficients on the building energy consumption in urban neighborhoods with different plan area densities. Energ Build 2015;86(0):449–63.
[30] Cheng H, Hayden P, Robins AG, Castro IP. Flow over cube arrays of different packing densities. J Wind Eng Ind Aerodyn 2007;95(8):715–40.
[31] Heidarinejad M. Relative significance of heat transfer processes to quantify tradeoffs between complexity and accuracy of energy simulations with a building energy use patterns classification. Mechanical Engineering, Pennsylvania State University; 2014.
[32] EnergyPlus. EnergyPlus engineering reference. 2013.
[33] Hargreaves DM, Wright NG. On the use of the k– model in commercial CFD software to model the neutral atmospheric boundary layer. J Wind Eng Ind Aerodyn 2007;95(5):355–69.
[34] Tominaga Y, Mochida A, Yoshie R, Kataoka H, Nozu T, Yoshikawa M, et al. AIJ guidelines for practical applications of CFD to pedestrian wind environment around buildings. J Wind Eng Ind Aerodyn 2008;96(10–11):1749–61.
[35] Franke J, Sturm M, Kalmbach C. Validation of OpenFOAM 1.6.x with the German VDI guideline for obstacle resolving micro-scale models. J Wind Eng Ind Aerodyn 2012;104–106(0):350–9.
[36] Srebric J, Heidarinejad M, Liu J. Building neighborhood emerging properties and their impacts on multi-scale modeling of building energy and airflows. Build Environ 2015 (Accepted).
[37] Liu J, Srebric J, Yu N. A rapid and reliable numerical method for predictions of outdoor thermal environment in actual urban areas. In: ASME 2013 summer heat transfer Conference, HT 2013 (Invited paper). Minneapolis, MN: ASME; 2013. p. 1–14. Paper No. HT2013-17782, pp. V003T21A008.
[38] Grimmond CSB, Cleugh HA, Oke TR. An objective urban heat storage model and its comparison with other schemes. Atmos Environ Part B Urban Atmos 1991;25(3):311–26.
[39] Roache PJ. Perspective: a method for uniform reporting of grid refinement studies. J Fluids Eng 1994;116(3):405–13.
[40] Bruelisauer M, Meggers F, Saber E, Li C, Leibundgut H. Stuck in a stack—Temperature measurements of the microclimate around split type condensing units in a high rise building in Singapore. Energ Build 2014;71(0):28–37.
[41] Variable rate rooftop unit test (VRTUT) report. Vancouver, WA: New Buildings Institute; 2013.
[42] Avara A, Daneshgar E. Optimum placement of condensing units of split-type air-conditioners by numerical simulation. Energ Build 2008;40(7):1268–72.
[43] Bojic M, Lee M, Yik F, Burnett J. Influence of clearances on the energy performance of window-type air-conditioners at the same level outside residential buildings. Build Environ 2002;37(7):713–26.
[44] OpenStudio 1.1.0. National Renewable Energy Laboratory; 2013.
[45] Lawrence Berkeley National Laboratory EnergyPlus Version 8.0. UIUC Building Systems Laboratory; 2013.
[46] Deru M, Field K, Studer D, Benne K, Griffith B, Torcellini P, et al. U.S. Department of energy commercial reference building models of the national building stock. NREL; 2011.
[47] BCL. Building component library (BCL). National Renewable Energy Laboratory (NREL); 2014.